COMMUNICATION

Check for updates

Stable and efficient rare-earth free phosphors based on an Mg(II) metal–organic framework for hybrid light-emitting diodes†

Youssef Atoini, [ID] *‡[a] Luca M. Cavinato,‡[a] Jean-Louis Schmitt, [ID] [b] Daniel Van Opdenbosch[c] and Rubén D. Costa [ID] *[a]

Stable and efficient green hybrid light-emitting diodes (HLEDs) were fabricated from a highly emissive Mg(II)-tetraphenyl ethylene derivative metal–organic framework embedded in a polystyrene matrix (Mg-TBC MOF@PS). The photoluminescence quantum yield (ϕ) of the material, >80%, remains constant upon polymer embedment. The resulting HLEDs featured high luminous efficiencies of >50 lm W^{-1} and long lifetimes of >380 h, making them among the most stable MOF-based HLEDs. The significance of this work relies on the combination of many features, such as the abundance of the metal ion, the straightforward scalability of the synthetic protocol, the great ϕ reached upon phosphor fabrication, and the state-of-the-art HLED performances.

Commercial light-emitting diodes (LEDs) consist of a stable UV- or blue-emitting pumping chip covered by a colour down-converting filter, or an inorganic phosphor (IP), that is mainly based on rare-earth elements (*e.g.*, Ce^{3+} and Eu^{3+}) or CdSe quantum dots. Such materials are undesirable as they do not fulfil the current ecologically friendly- and cost-related needs. This issue has driven the research community to actively look for alternatives using organic phosphors (OPs) in the next generation of so-called hybrid LEDs (HLEDs).[1,2] They combine the highly efficient and stable inorganic LED chip with an organic colour down-converting filter prepared by embedding emitting species, such as organic molecules,[3,4] coordination complexes,[5,6] metal-organic frameworks (MOFs),[5,7] and/or bio-derived materials,[8,9] in organic polymeric matrices (*e.g.*, poly-

methylmethacrylate,[10] polystyrene (PS),[7] polycarbonate,[11] polyethylene oxide (PEO),[12] and hydroxypropyl cellulose[13]). Regarding MOFs, they are coordination polymers made of one or several organic moiety(ies) called ligand(s) or linker(s) coordinated to one or several metal ion(s) or metallic cluster(s) called node(s).[14,15] The repetition between the node(s) and the linker(s) forms a geometrically well-defined, highly crystalline, and porous structure. MOFs are considered as rising materials in various research fields, such as catalysis,[16,17] gas storage,[18,19] gas separation,[20,21] sensing,[22,23] and, to a lesser extent, optoelectronics[24–27] and information encryption.[28,29]

This is attributable to their straightforward syntheses, large surface area, tuneable porosity, high degree of crystallinity, and possibility of post-synthetic modification by guest insertion. In addition, luminescent MOFs feature interesting photophysical properties, resulting from ligand centred (LC)/metal-to-ligand charge transfer transitions.[30,31] Thus, they were already employed to fabricate HLEDs, but without solving critical issues related to either (i) the use of expensive and polluting materials or (ii) the moderate device performance.[32–34] For instance, one of the best performing HLEDs involving an Earth-abundant MOF (*i.e.*, a Zn(II)-based MOF) embedded in a polyurethane matrix has shown an interestingly high luminous efficiency of 60 lm W^{-1}.[35] However, the stability was not disclosed.

Herein, we present a novel green HLED made from a highly emissive, rare-earth free and cost-effective MOF embedded in PS. The MOF (**Mg-TBC MOF**) bears a tetradentate linker, namely 4′,4‴,4‴‴,4‴‴‴-(ethene-1,1,2,2-tetrayl)tetrakis(([1,1′-biphenyl]-4-carboxylic acid)) (**TBC**), and an Mg(II) ion as a node. Besides the rare-earth free aspect of the phosphor, the HLED simultaneously achieved a high efficiency of 50 lm W^{-1} in concert with an operation stability of 16 days.

A tetraphenylethylene (TPE) scaffold was selected as a linker due to the high quantum yield of TPE-based MOFs, with different nodes such as Eu^{3+}, Zn^{2+}, Cd^{2+}, and Gd^{3+}.[36–39]

TBC was synthesised according to three steps (Scheme S1, more details in the ESI†).[40] The ligand and its synthetic intermediates were characterised by nuclear magnetic resonance

[a]*Technical University of Munich, Campus Straubing for Biotechnology and Sustainability, Chair of Biogenic Functional Materials, Schulgasse, 22, Straubing 94315, Germany. E-mail: y.atoini@tum.de, ruben.costa@tum.de*
[b]*Laboratoire de Chimie Supramoléculaire, Institut de Science et d'Ingénierie Supramoléculaires, 8, allée Gaspard Monge, 67000 Strasbourg, France*
[c]*Technical University of Munich, Campus Straubing for Biotechnology and Sustainability, Chair for Biogenic Polymers, Schulgasse, 22, Straubing 94315, Germany*

(NMR) spectroscopy and electrospray ionisation high-resolution mass spectrometry (ESI HR-MS) (Fig. S1–S3†). The **Mg-TBC MOF** was synthesised using **TBC** as a linker and $MgCl_2$ as the node's precursor under solvothermal conditions (Fig. 1, *cf.* the ESI† for more details).

They were subsequently characterised by several techniques. Among them, PXRD reveals a crystalline material, typical of MOFs, and the space group and the dimensions of the unit cell were determined by indexing and refinement processes, as shown in Fig. S4.† From the space group and the dimensions of the unit cell, we could successfully generate a calculated pattern, and interestingly the difference between the measured and calculated patterns is a *quasi*-flat line (*cf.* Fig. S4†). Moreover, the low R_{wp} value found resulting from the fitting, 9.3, points out the crystallinity of the material. The material indeed crystallises in a triclinic unit cell ($P\bar{1}$, a, b, c (Å) = 10.55, 17.24, and 21.63, respectively; α, β, γ (°) = 102.37, 92.72, and 95.72, respectively). Scanning electron microscopy (SEM) images were additionally recorded, emphasising the crystalline nature of the **Mg-TBC MOF**. Indeed, the micrographs, depicted in Fig. S4,† show crystalline structures in the range of several micrometres. Nitrogen adsorption–desorption experiments provided information about the surface area and the pore size, 340 m^2 g^{-1} and 1.9 nm, respectively (Fig. S5†). Furthermore, thermogravimetric analysis (TGA) was conducted in order to determine the thermal stability of the material (Fig. S6†). This analysis indicates two main weight decreases. In detail, a first drop, up to 200 °C, was observed and attributed to the loss of solvent molecules present in the MOF cavities, *i.e.* ethanol (used for the purification process – Soxhlet extraction) and dimethylformamide (used for the synthesis process). A second drop, between 500 °C and 600 °C, was noted and attributed to the ligand decomposition. The thermal stability of alike MOFs was also studied, showing similar results.[7,40]

The photophysical properties of the **Mg-TBC MOF** were studied, as depicted in Fig. 2 and Table 1. The emission in the powder state shows a broad, featureless spectrum centred at 523 nm (full width at half maximum, FWHM: 106 nm), with a high photoluminescence quantum yield (ϕ) of 81% and an excited-state lifetime (τ) of 3.96 ns, indicating a fluorescence behaviour attributed to a ligand centred (LC) emission (*cf.* Fig. S7† for the emission and the excitation spectra of TBC in the powder state and Fig. S8† for the decay plots). However, it is important to note that the ϕ of the **TBC** ligand alone is 30%.[40] This nicely points out the need for the metal cation to decrease the flexibility of the ligand conformation, therefore
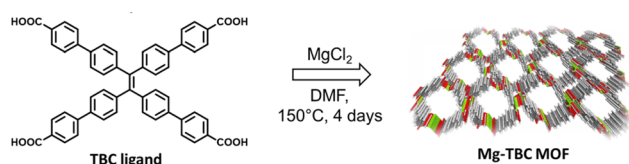

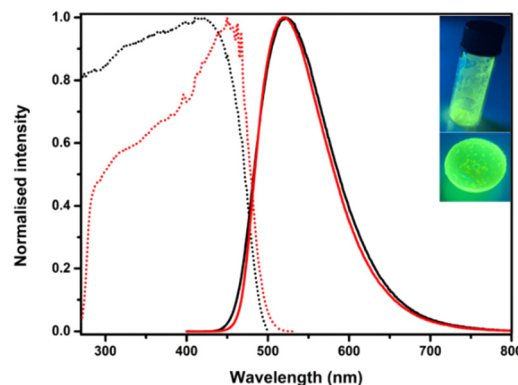**Fig. 2** Excitation (dotted line, λ_{Em} = 523 nm) and emission (full line, λ_{Exc} = 370 nm) spectra of the **Mg-TBC MOF** in the powder state (black) and **Mg-TBC MOF@PS** (red). Inset: top: pictures of the **Mg-TBC MOF** in the powder state; bottom: picture of **Mg-TBC MOF@PS**.

Table 1 Photophysical properties of **TBC**, **Mg-TBC MOF**, in the powder state embedded in PS as a coating, and *post-mortem* (λ_{Exc} = 370 nm)

Sample	λ_{Em} (nm)	FWHM (nm)	ϕ (%)	τ (ns)	k_r (s^{-1})	k_{nr} (s^{-1})
TBC	541	94	30	3.88	7.73×10^7	1.80×10^8
Mg-TBC MOF powder	523	106	81	3.96	2.23×10^8	5.59×10^7
Mg-TBC MOF@PS	522	102	83	3.87	2.35×10^8	3.83×10^7
Mg-TBC MOF *post-mortem*	545	120	5	3.1	1.61×10^7	4.45×10^7

decreasing the non-radiative pathways. In other words, even though the emission is located on the **TBC** linker, the presence of Mg(II) ions as a node is crucial in order to achieve outstanding luminous output, highlighting the synergistic effect between the linker and nodes.[27,40] According to the work of Omary, Zhou and coworkers, the origin of this increase is due to limited inter- and intramolecular interactions, as well as framework rigidity.[40] Furthermore, to rule out the effect of the solvent molecules that could have possibly remained inside the pores of the **Mg-TBC MOF**, a high vacuum (<0.1 mbar) was applied together with a moderately high temperature (60 °C) overnight. The luminescence properties were tested, as depicted in Fig. S9,† and were compared to the as-synthesised MOFs. Interestingly, both samples feature identical properties.

With regard to their use as colour down-converting filters, an OP (thickness: 1.61 ± 0.05 mm) was prepared by embedding the **Mg-TBC MOF** in a PS matrix (**Mg-TBC MOF@PS**, see the ESI† for the embedding process protocol). The photophysical properties of this coating were investigated (Fig. 2 and Table 1), pointing out similarities between those of both **Mg-TBC MOF@PS** (λ_{Em} = 522 nm, FWMH = 102 nm) and **Mg-TBC MOF** in the powder state (*vide supra*), while ϕ remains similar, meaning that the PS matrix does not affect the luminescence of the material. Finally, the τ value holds at 3.87 ns, indicating the same nature of the excited state (LC) and the fluorescence mechanism. To rule out the effect of the concentration of the MOF dispersed inside PS, two additional MOF : PS ratios were

**Fig. 1** Synthesis scheme of the **Mg-TBC MOF**.

studied, one with 3 times less MOF (**Mg-TBC MOF/3@PS**) and another with 6 times less MOF (**Mg-TBC MOF/6@PS**), with the amount of PS remaining constant (*cf.* Fig. S10†). The luminescence properties of the coatings based on these two materials are very similar to those of **Mg-TBC MOF@PS**, indicating that the coatings do not either suffer or benefit from different dispersion concentrations.

Next, HLEDs were fabricated using a commercial 380 nm chip covered by a **Mg-TBC MOF@PS** coating using an on-chip configuration (*i.e.*, with the coating directly placed on top of the chip).[7,41] More details on the HLEDs fabrication are reported in the ESI.† At first, the *Commission Internationale de l'Eclairage* (CIE) coordinates were determined, featuring *x*, *y* coordinates of 0.32, 0.57 (*cf.* Fig. 3, top). Additionally, device stability was investigated under ambient conditions at high applied currents, *i.e.* 200 mA. Interestingly, the HLEDs feature quantitative photoconversion, and this information provides evidence of satisfactory efficiency (*vide infra*). The device's stability was determined by $T_{1/2}$, *i.e.* the time needed to reach half of its initial intensity. Under these conditions, $T_{1/2}$ of the HLEDs was found to be 11 h (*cf.* Fig. 3, top), which is associated with a drastic increase in temperature (maximum device temperature: 91 °C), suggesting an important thermal quenching as an OP degradation mechanism. To elucidate whether an additional photo-induced oxidation process is responsible for the OP degradation or not, the same experiment was performed under a dry nitrogen atmosphere. Strikingly, the sample appears to be much more stable than in air, which provides evidence of the photooxidation of the sample.

Indeed, at high photon flux (200 mA) and following an on-chip configuration, the sample only lost 5% of its initial intensity after 11 h (*cf.* Fig. S11†), whereas within the same period of time and according to the same conditions, the sample under an ambient atmosphere loses 50% of its initial intensity (Fig. 3). The photooxidation of the ligand is here attributed to a decarboxylation mechanism,[42,43] and the CO_2 release is likely responsible for the high device temperature. Concurrently, HLED emission spectra were recorded over time, as displayed in Fig. 3, bottom. Notably, only a very slight bathochromic shift was noted (5 nm) within 72 h.

However, a non-negligible broadening of the emission signal evolved over time, in which the spectrum at t_0 and that at 72 h present a FWHM of 85 nm and 104 nm, respectively. This broadening is also accompanied by the appearance, after 2 h, of a broad shoulder at around 565 nm. As a means to have a better understanding of the degradation process, the **Mg-TBC MOF**, in the powder state, was exposed to the same UV pumping chip for one week at 200 mA. This "*post-mortem*" sample was analysed by PXRD and photophysical characterisation. Noteworthily, the PXRD pattern of the "*post-mortem*" powder shows an amorphous structure, referring to the degradation of the MOF. This was further supported by photoluminescence characterisation (*cf.* Fig. S12†). Firstly, a bathochromic shift and broadening of the emission spectrum (λ_{Em} = 545 nm, FWHM = 120 nm) were noted, reflecting the electroluminescence behaviour of the coating. This is associated with a significant decrease in ϕ and a shortening of τ, (5% and 3.1 ns, respectively, *cf.* Table 1). These are in perfect agreement with the above-discussed changes in the electroluminescence spectra. It is important to note that the amorphous nature of the PS matrix hampered the ability to obtain meaningful data in the *post-mortem* colour down-converting material. Additionally, in order to gain more insight into our previous statement, that is the Mg(II) ion provides more rigidity and stability to the MOF, a coating prepared from the TBC ligand alone was prepared and a degradation experiment of TBC at 200 mA was conducted on-chip, and the low stability of the sample, $T_{1/2}$ = *ca.* 15 min, (*cf.* Fig. S14†) confirms the importance of Mg(II) in the rigidification process of the MOF. At this point, the optimal applied current ranging from 10 mA to 200 mA in terms of device efficiency was investigated. While the external quantum efficiency (EQE) reached a maximum value of 23% at 20 mA (*cf.* Fig. S14†), the luminous efficiency peaks at 50 lm W^{-1} at a similar current (Fig. 4, top). These strikingly high-efficiency values indicate exceptionally efficient HLEDs, with respect to several previous works.[32–34] Thus, further tests under continuous irradiation at 20 mA were conducted, reaching $T_{1/2}$ values of 385 h, that is 16 days (*cf.* Fig. 4, middle and bottom). This outstanding stability, combined with the high efficiency and the material's eco-friendliness, undoubtedly indicates the formation of a competitive and promising MOF-based HLED.
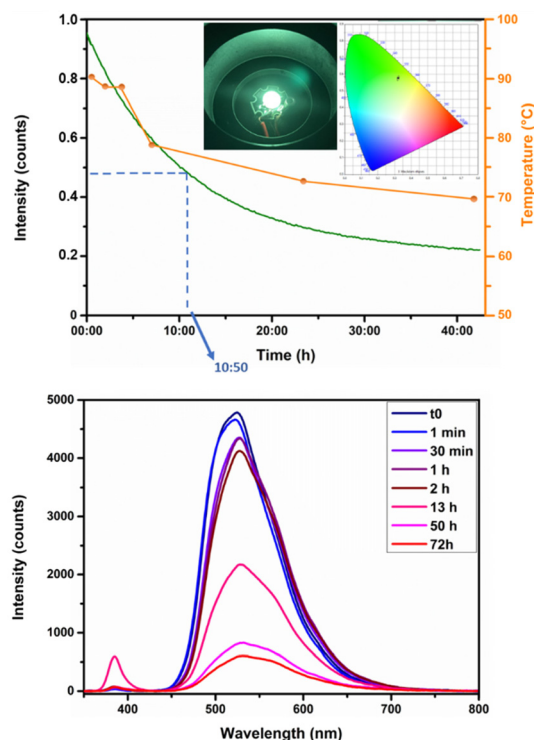
Fig. 3 Top: emission intensity over time and temperature evolution of the **Mg-TBC MOF**-based HLED in an on-chip configuration at 200 mA. The stability of the HLED is here defined by $T_{1/2}$. Inset: picture and chromaticity diagram of the device; bottom: electroluminescence spectra at different device running times: from t_0 to 72 h.
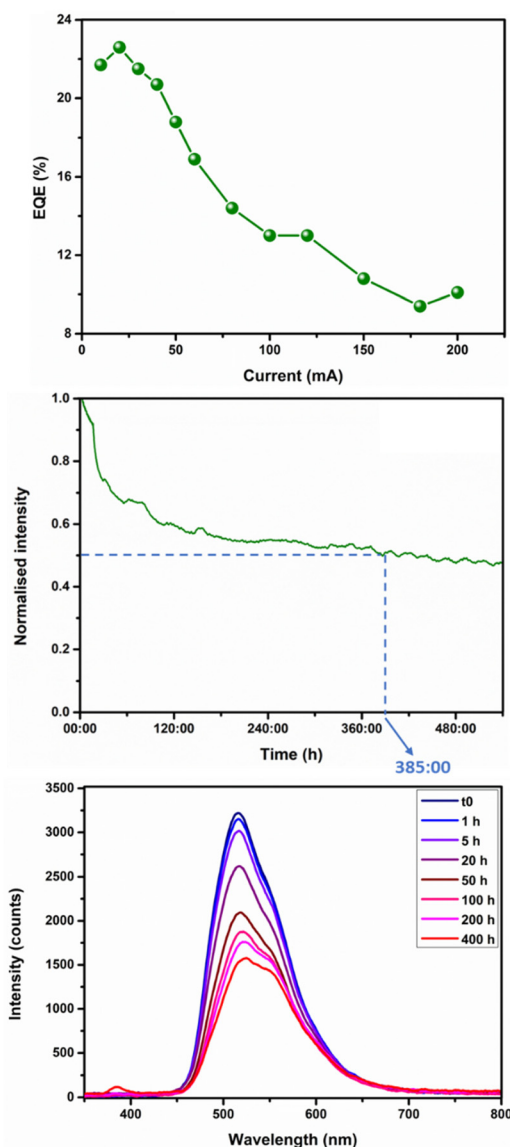
Fig. 4 Top: luminous efficiency *vs.* applied current from 10 mA to 200 mA; middle: emission intensity over time of the **Mg-TBC MOF**-based HLED in an on-chip configuration at 20 mA. The stability of the HLED is here defined by $T_{1/2}$; bottom: electroluminescence spectra at different device running times at 20 mA: from t_0 to 400 h.

Conclusions

To conclude, we describe the synthesis and characterisation of a highly emissive and rare-earth free MOF with an outstanding green emission. While the emitting excited state is located at the linker, as attested by its nanosecond-range τ, the metallic node allows a ligand rigidification that leads to an almost 3-fold enhancement of ϕ. What is more, this figure reached values of up to 83% in colour-converting filters prepared with PS. Subsequently, HLEDs were fabricated, showing a high device stability of 16 days associated with a device efficiency of 50 lm W^{-1} or 23%.

Finally, we could elucidate the nature of the degradation process, attributed to the photooxidation of the ligand, and consequently an increase in device temperature. This work undoubtedly strengthens this cutting-edge field, paving the way for new generations of greener OPs based on more environmentally friendly MOFs towards monochromatic and white HLEDs.

Data availability

The datasets supporting this article have been uploaded as part of the ESI.†

Conflicts of interest

There are no conflicts to declare.

Acknowledgements

References

1 M.-S. Wang and G.-C. Guo, *Chem. Commun.*, 2016, **52**, 13194.
2 Y. Huang, T. A. Cohen and C. K. Luscombe, *Adv. Sustainable Syst.*, 2022, **6**, 2000300.
3 J. He, S. Yang, K. Zheng, Y. Zhang, J. Song and J. Qu, *Green Chem.*, 2018, **20**, 3557.
4 N. J. Findlay, J. Bruckbauer, A. R. Inigo, B. Breig, S. Arumugam, D. J. Wallis, R. W. Martin and P. J. Skabara, *Adv. Mater.*, 2014, **26**, 7290.
5 C.-Y. Sun, X.-L. Wang, X. Zhang, C. Qin, P. Li, Z.-M. Su, D.-X. Zhu, G.-G. Shan, K.-Z. Shao, H. Wu and J. Li, *Nat. Commun.*, 2013, **4**, 2717.
6 Y.-W. Zhao, F.-Q. Zhang and X.-M. Zhang, *ACS Appl. Mater. Interfaces*, 2016, **8**, 24123.
7 Y. Atoini, L. M. Cavinato, J. Fernandez-Cestau, Y. Gmach, D. Van Opdenbosch and R. D. Costa, *Adv. Opt. Mater.*, 2023, **11**, 2202643.
8 S. Ferrara, J.-P. Fernández-Blázquez, J.-P. Fuenzalida Werner and R. D. Costa, *Adv. Funct. Mater.*, 2023, **33**, 2300350.
9 L. Niklaus, H. Dakhil, M. Kostrzewa, P. B. Coto, U. Sonnewald, A. Wierschem and R. D. Costa, *Mater. Horiz.*, 2016, **3**, 340.
10 D. Di Martino, L. Beverina, M. Sassi, S. Brovelli, R. Tubino and F. Meinardi, *Sci. Rep.*, 2014, **4**, 4400.
11 T. Güner, D. Köseoğlu and M. M. Demir, *Opt. Mater.*, 2016, **60**, 422.

12 M. Nieddu, M. Patrian, S. Ferrara, J. P. Fuenzalida Werner, F. Kohler, E. Anaya-Plaza, M. A. Kostiainen, H. Dietz, J. R. Berenguer and R. D. Costa, *Adv. Sci.*, 2023, **10**, 2300069.

13 M. Hasler, M. Patrian, J. A. Banda-Vázquez, S. Ferrara, A. C. Stiel, J. Fuenzalida-Werner and R. D. Costa, *Adv. Funct. Mater.*, 2023, 2301820.

14 H. Li, M. Eddaoudi, M. O'Keeffe and O. M. Yaghi, *Nature*, 1999, **402**, 276.

15 J. L. C. Rowsell and O. M. Yaghi, *Microporous Mesoporous Mater.*, 2004, **73**, 3.

16 V. Pascanu, G. González Miera, A. K. Inge and B. Martín-Matute, *J. Am. Chem. Soc.*, 2019, **141**, 7223.

17 Y.-S. Wei, M. Zhang, R. Zou and Q. Xu, *Chem. Rev.*, 2020, **120**, 12089.

18 D. Alezi, Y. Belmabkhout, M. Suyetin, P. M. Bhatt, Ł. J. Weseliński, V. Solovyeva, K. Adil, I. Spanopoulos, P. N. Trikalitis, A.-H. Emwas and M. Eddaoudi, *J. Am. Chem. Soc.*, 2015, **137**, 13308.

19 J. A. Mason, M. Veenstra and J. R. Long, *Chem. Sci.*, 2014, **5**, 32.

20 Q. Qian, P. A. Asinger, M. J. Lee, G. Han, K. Mizrahi Rodriguez, S. Lin, F. M. Benedetti, A. X. Wu, W. S. Chi and Z. P. Smith, *Chem. Rev.*, 2020, **120**, 8161.

21 Z. Kang, L. Fan and D. Sun, *J. Mater. Chem. C*, 2017, **5**, 10073.

22 L. E. Kreno, K. Leong, O. K. Farha, M. Allendorf, R. P. Van Duyne and J. T. Hupp, *Chem. Rev.*, 2012, **112**, 1105.

23 H.-Y. Li, S.-N. Zhao, S.-Q. Zang and J. Li, *Chem. Soc. Rev.*, 2020, **49**, 6364.

24 V. Stavila, A. A. Talin and M. D. Allendorf, *Chem. Soc. Rev.*, 2014, **43**, 5994.

25 B. Zhou, Z. Qi and D. Yan, *Angew. Chem., Int. Ed.*, 2022, **61**, e202208735.

26 B. Zhou and D. Yang, *Chem. Sci.*, 2022, **13**, 7429.

27 H. Kaur, S. Sundriyal, V. Pachauri, S. Ingebrandt, K.-H. Kim, A. L. Sharma and A. Deep, *Coord. Chem. Rev.*, 2019, **401**, 213077.

28 Y.-J. Ma, G. Xiao, X. Fang, T. Chen and D. Yan, *Angew. Chem., Int. Ed.*, 2023, **62**, e202217054.

29 S. Liu, Y. Lin and D. Yan, *Sci. Bull.*, 2022, **67**, 2076.

30 M. D. Allendorf, C. A. Bauer, R. K. Bhakta and R. J. T. Houk, *Chem. Soc. Rev.*, 2009, **38**, 1330.

31 B. Zhou and D. Yang, *Adv. Funct. Mater.*, 2023, **33**, 2300735.

32 E. Angioni, R. J. Marshall, N. J. Findlay, J. Bruckbauer, B. Breig, D. J. Wallis, R. W. Martin, R. S. Forgan and P. J. Skabara, *J. Mater. Chem. C*, 2019, **7**, 2394.

33 A. Wang, Y.-L. Hou, F. Kang, F. Lyu, Y. Xiong, W.-C. Chen, C.-S. Lee, Z. Xu, A. L. Rogach, J. Lu and Y. Y. Li, *J. Mater. Chem. C*, 2019, **7**, 2207.

34 Y. Tang, H. Wu, W. Cao, Y. Cui and G. Qian, *Adv. Opt. Mater.*, 2021, **9**, 2001817.

35 E. Angioni, R. J. Marshall, N. J. Findlay, J. Bruckbauer, B. Breig, D. J. Wallis, R. W. Martin, R. S. Forgan and P. J. Skabara, *J. Mater. Chem. C*, 2019, **7**, 2394.

36 K. J. Stawiasz, J. I. Deneff, R. A. Reyes, T. J. Woods, L. E. S. Rohwer, N. Valdez, M. A. Rodriguez, A. Lawal, J. S. Moore and D. F. Sava Gallis, *CrystEngComm*, 2023, **25**, 2701.

37 N. B. Shustova, B. D. McCarthy and M. Dincă, *J. Am. Chem. Soc.*, 2011, **133**, 20126.

38 S. Wang, L. Zhao, H. Sun, Y. Wu, R. Wang, S. Zhang, L. Du and Q.-H. Zhao, *Chem. – Eur. J.*, 2022, **28**, e202202154.

39 S. Mao, S. Lin, X. Li and H. Wang, *Cryst. Growth Des.*, 2022, **22**, 5791.

40 Z. Wei, Z.-Y. Gu, R. K. Arvapally, Y.-P. Chen, R. N. McDougald Jr., J. F. Ivy, A. A. Yakovenko, D. Feng, M. A. Omary and H.-C. Zhou, *J. Am. Chem. Soc.*, 2014, **136**, 8269.

41 S. Ferrara, S. H. Mejias, M. Liutkus, G. Renno, F. Stella, I. Kociolek, J. P. Fuenzalida-Werner, C. Barolo, P. B. Coto, A. L. Cortajarena and R. D. Costa, *Adv. Funct. Mater.*, 2022, **32**, 2111381.

42 L. Candish, M. Freitag, T. Gensch and F. Glorius, *Chem. Sci.*, 2017, **8**, 3618.

43 T. Charbouillot, S. Gorini, G. Voyard, M. Parasolz, M. Brigante, L. Deguillaume, A.-M. Delort and G. Mailhot, *Atmos. Environ.*, 2012, **56**, 1.